

Effects of microstructure on flow properties of fibrous porous media at moderate Reynolds number

A. Tamayol,* K. W. Wong, and M. Bahrami

Mechatronics Systems Engineering, School of Engineering Sciences, Simon Fraser University, BC, Canada V3T0A3

(Received 11 January 2011; published 27 February 2012)

In this study, effects of microstructure on the viscous permeability and Forchheimer coefficient of monodispersed fibers are investigated. The porous material is represented by a unit cell which is assumed to be repeated throughout the medium. Based on the orientation of the fibers in the space, fibrous media are divided into three categories: one-, two-, and three-directional (1D, 2D, and 3D) structures. Parallel and transverse flow through square arrangements of 1D fibers, simple 2D mats, and 3D simple cubic structures are solved numerically over a wide range of porosity ($0.35 < \varepsilon < 0.95$) and Reynolds number ($0.01 < Re < 200$). The results are used to calculate the permeability and the inertial coefficient of the considered geometries. An experimental study is performed; the flow coefficients of three different ordered tube banks in the moderate range of Reynolds number ($0.001 < Re < 15$) are determined. The numerical results are successfully compared with the present and the existing experimental data in the literature. The results suggest that the permeability and Forchheimer coefficient are functions of porosity and fiber orientation. A comparison of the experimental and numerical results with the Ergun equation reveals that this equation is not suitable for highly porous materials. As such, accurate correlations are proposed for determining the Forchheimer coefficient in fibrous porous media.

DOI: 10.1103/PhysRevE.85.026318

PACS number(s): 47.56.+r, 47.15.-x

I. INTRODUCTION

An in-depth understanding of flow through fibrous porous materials and determining the resulting pressure drop are important in numerous engineering applications such as filtration and separation of particles [1], biological systems [2], composite fabrication [3], compact heat exchangers [4–6], biological materials [7], and fuel cell technology [8]. In creeping flow regime, according to the Darcy equation, the relationship between volume-averaged velocity through porous media, U_D , and the pressure drop is linear [9]:

$$-\frac{dP}{dx} = \frac{\mu}{K} U_D, \quad (1)$$

where K is the permeability. In higher Reynolds numbers, the relationship becomes nonlinear and a modified Darcy equation should be used [9]:

$$-\frac{dP}{dx} = \frac{\mu}{K} U_D + \beta U_D^2, \quad (2)$$

where β is called the inertial coefficient. For a fibrous medium, the flow coefficients are expected to depend on the porosity, fiber diameter, distribution of fibers in the space, and the orientation of fibers relative to the flow direction.

Based on the orientation of the fibers in space, three categories can be considered for fibrous structures (Fig. 1): one-directional (1D), where the axes of fibers are parallel to each other; two-directional (2D), where the fiber axes are located on planes parallel to each other with an arbitrary distribution on these planes; and three-directional (3D), where the fiber axes are randomly positioned and oriented in a given volume. With the exception of the 3D structures, the rest are anisotropic [10].

A variety of analytical, theoretical, and experimental methods have been employed by researchers to predict the flow properties of fibrous materials. Existing analytical works are mostly limited to study of the creeping flow over a single cylinder with a limited boundary layer or through periodic fiber arrays [11–18]. In addition, few models have been reported that are capable of predicting the permeability of 2D and 3D structures [1, 19–22]; recently, Tamayol and Bahrami [22] have reviewed these models. Numerical and experimental studies for creeping flow in fibrous media covers a wider range of porosity and fiber distribution in 1D [21, 23, 24], 2D [21, 25–29], and 3D [30–33] structures. Most of the existing correlations in literature for 2D and 3D are based on curve fitting of numerical and experimental data [10].

Considering the inertial effects in the flow analysis adds to the complexity of the problem. As such, no analytical solutions were found in the literature for the moderate Reynolds number flows through fibrous structures. The existing studies are either numerical or experimental. Effects of Reynolds number on the pressure drop through unidirectional monodisperse and bimodal 1D fibrous structures were investigated numerically by Nagelhout *et al.* [34], Martin *et al.* [35], Lee and Yang [36], Koch and Ladd [37], Edwards *et al.* [38], Ghaddar [39], and Papathanasiou *et al.* [40]. Their results, in general, confirmed a parabolic relationship between pressure drop and flow rate in the considered geometries. However, comparison of these numerical results with conventional models in the literature such as the Ergun equation was not successful [40].

The studies of moderate Reynolds number flows through 2D and 3D structures are not frequent. Recently, Rong *et al.* [41] used the lattice Boltzmann method to investigate the flow in a three dimensional random fiber network with porosities in the range of $0.48 < \varepsilon < 0.72$. Their results were in agreement with the Forchheimer equation which is in line with the observations of [40]. Boomsma *et al.* [42] have also studied flow in high porosity 3D fibrous structures to predict flow properties of open cell aluminum foams.

*Corresponding address: Mechatronics Systems Engineering, Simon Fraser University, 4300, 250–13450 102nd Avenue, Surrey, BC, Canada, V3T0A3; ali.tamayol@sfu.ca

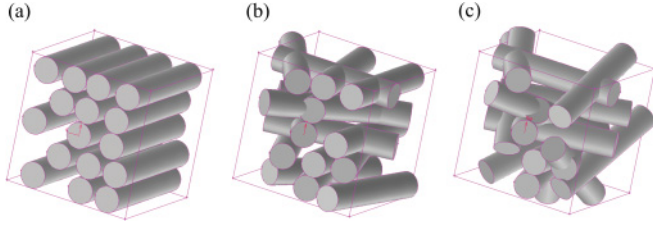


FIG. 1. (Color online) Structures with different fibers orientation; (a) 1D, (b) 2D, and (c) 3D.

Our literature review revealed that no comprehensive studies exist on the effects of microstructure, especially fiber orientation, on the flow properties of fibrous materials in a low to moderate range of Reynolds numbers. In addition, very few experimental works have been published for the flow through ordered fibers with moderate Reynolds numbers. In this study, the effects of porosity and fiber orientation on the flow coefficients of monodispersed fibrous materials are investigated. Parallel and transverse flow through a variety of fibrous matrices including square fiber arrangements, simple two directional mats, and simple cubic structures are solved numerically over the porosity range of $0.4 < \varepsilon < 0.95$ and Reynolds number range of $0.01 < Re < 200$. The results are then used to find permeability and the inertial coefficient of the solid matrices. To verify the present numerical results, pressure drop through three different tube banks with porosity range of $0.8 < \varepsilon < 0.9$ are tested using various water-glycerol mixtures to determine the flow coefficients. The numerical results are successfully compared with the present experimental measurements and the data found in the literature.

II. GEOMETRICAL MODELING

Following other researchers [19–22,34–40,43–45], the porous media are represented by a unit cell which is assumed to be repeated throughout the media. The unit cell (or basic cell) is the smallest volume which can represent the characteristics of the whole medium.

The flow properties of square arrays of equally sized, equally spaced fibers, shown in Fig. 2, are studied as a representative of 1D structures. The solid volume fraction φ for the arrangement shown in Fig. 2 is related to the distance between the centers of adjacent fibers, S , and the fibers diameter d :

$$\varphi = \frac{\pi d^2}{4S^2}. \quad (3)$$

To model 2D woven textile materials, the ordered geometry shown in Fig. 3, where the fibers are resting on each other,

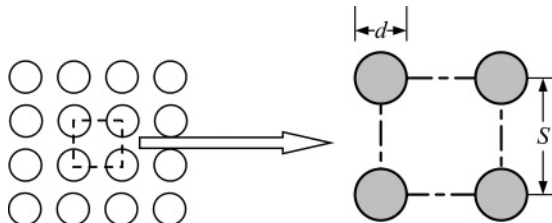


FIG. 2. Square fiber arrangement for analysis of 1D structures.

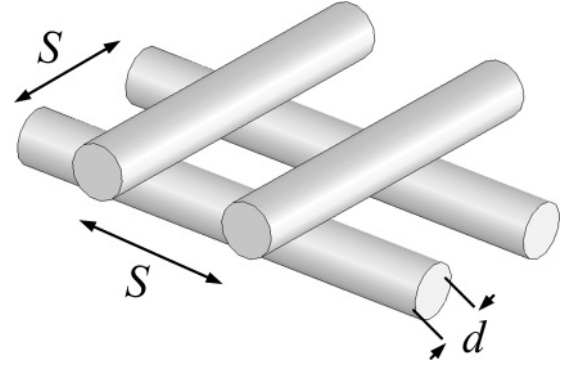


FIG. 3. Considered unit cells for modeling 2D fibrous structures.

is considered. The relationship between solid volume fraction (φ) and other geometrical parameters in Fig. 3 is

$$\varphi = \frac{\pi d}{4S}. \quad (4)$$

The flow properties of simple cubic (SC) structures are investigated as a representative unit cell for 3D materials; see Fig. 4. The relationship between the solid volume fraction and geometric parameters of SC arrangement is [32]

$$\varphi = \frac{3\pi d^2}{4S^2} - \sqrt{2} \frac{d^3}{S^3}. \quad (5)$$

III. MICROSCOPIC AND MACROSCOPIC FLOW EQUATIONS

If the pore sizes are much larger than the molecular mean free path, flow in pore scale is governed by the Navier-Stokes equation; that is the continuum flow hypothesis which is considered here. Assuming incompressible, steady state flow, the microscopic equations become [9]

$$\vec{\nabla} \cdot \vec{V} = 0, \quad (6)$$

$$\rho \vec{V} \cdot \nabla \vec{V} = -\vec{\nabla} P + \mu \vec{\nabla}^2 \vec{V}, \quad (7)$$

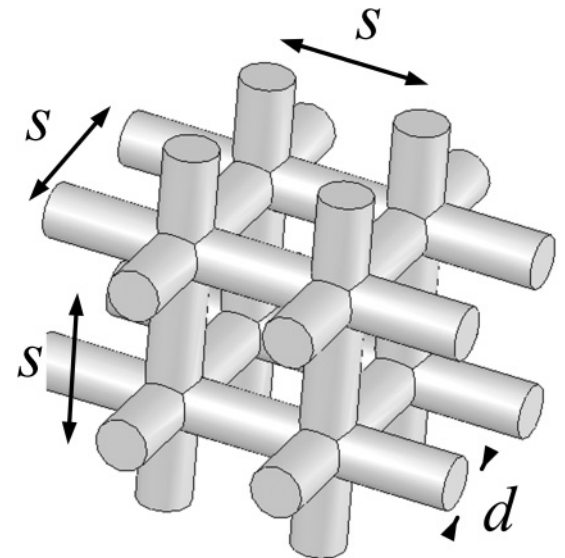


FIG. 4. Simple cubic unit cells for modeling 3D structures.

where \bar{V} is the pore scale velocity vector, and ρ and μ are the fluid density and viscosity, respectively. Equations (6) and (7) are subject to no-slip boundary condition at the fibers' surface. After volume averaging and some simplifications, Eq. (7) leads to Eq. (2), which is a decomposition of the viscous and inertial contributions. In the creeping flow limit, Eq. (2) reduces to Eq. (1). Equation (2) is usually written in the following form [9]:

$$-\frac{dP}{dx} = \frac{\mu}{K} U_D + \frac{\rho F}{\sqrt{K}} U_D^2, \quad (8)$$

where F is a dimensionless number called the Forchheimer coefficient. A special form of Eq. (6) is the Ergun equation:

$$-\frac{dP}{dx} = 150 \frac{(1-\varepsilon)^2}{\varepsilon^3 d^2} U_D + 1.75 \frac{(1-\varepsilon)}{\varepsilon^3 d} U_D^2, \quad (9)$$

where $K = \varepsilon^3 d^2 / 150(1-\varepsilon)^2$ and $F = 0.14/\varepsilon^{3/2}$. The Ergun equation is based on a curve fit of experimental data collected for granular materials [9].

IV. EXPERIMENTAL APPROACH

Experimental data for moderate Reynolds number flow through the fibrous structures of interest to us are not abundant in the open literature. As such, three samples of tube banks with 1D square arrangement shown in Fig. 5 were tested. To fabricate the tube bank sample, polymethyl methacrylate (PMMA) sheets of 3-mm thickness were cut and drilled using a laser cutter with an accuracy of 0.05 mm. Glass capillary tubes with diameter of 1.5 mm were inserted and fixed using an adhesive tape to form tube banks, as shown in Fig. 5. The lengths of the tube banks were selected such that a minimum of 15 rows of cylinders existed in the flow direction for each sample. The properties of the samples are summarized in Table I.

A custom-made gravity driven test bed, illustrated in Fig. 5, was built that included an elevated reservoir, an entry section, a sample holder section, and an exit section with a ball valve. The liquid level was kept constant during the experiment to ensure that the variation of the pressure head was negligible during the experiment. The pressure drop across the samples

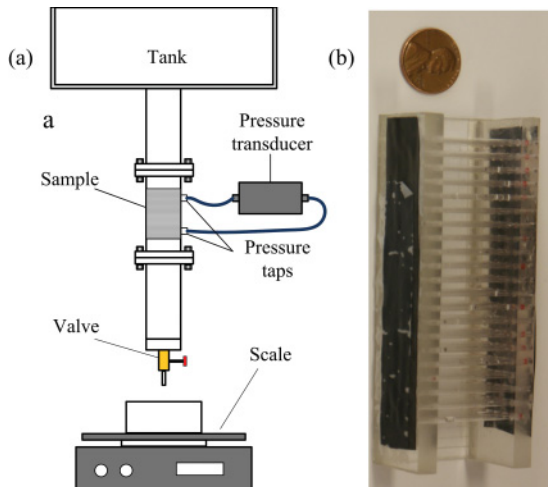


FIG. 5. (Color online) Schematic of the test setup.

TABLE I. Summary of the properties of the tested samples; water-glycol used as test fluid.

Sample name	ε	d (mm)	K (m ²)	β (m ⁻¹)	F
Sq-08	0.8	1.5	1.38×10^{-7}	75	0.028
Sq-085	0.85	1.5	3.74×10^{-7}	35.8	0.022
Sq-09	0.9	1.5	5.44×10^{-7}	26.7	0.020

was measured using a differential pressure transducer, PX-154 (BEC Controls). To minimize entrance and exit effects on the pressure drop measurements, pressure taps were located a few rows apart (at least three rows) from the first and the last tube rows in the tube bank samples. Several water-glycerol mixtures with different mass concentrations and viscosities (0.015–1.4 N s/m²) were used to change the flow Reynolds number from 0.001 to 15. The bulk flow was calculated by weighing the collected test fluid over a period of time. The maximum uncertainty in the flow rate measurements was 4%.

To obtain the permeability and the inertial coefficient from the measured pressure drop (dp/dx) and mass flow values, the volume-averaged superficial velocity U_D was calculated from the mass flow rate data and then $(dp/dx)/\mu U_D$ was plotted versus $\rho U_D/\mu$. The y intercept and the slope of the data were then $1/K$ and F/\sqrt{K} , respectively; see Eq. (8). Using Eq. (2), the inertial coefficient was then calculated. From Fig. 6, it can be seen that the measured pressure drops present a parabolic relationship with the volume-averaged velocity.

The uncertainty associated with the permeability and inertial coefficient, calculated based on the measured variables, can be estimated as

$$\frac{E(\beta, K)}{\beta, K} = \sqrt{\left[\frac{E(\rho U_D/\mu)}{\rho U_D/\mu} \right]^2 + \left[\frac{E(\Delta P/L\mu U_D)}{\Delta P/L\mu U_D} \right]^2}, \quad (10)$$

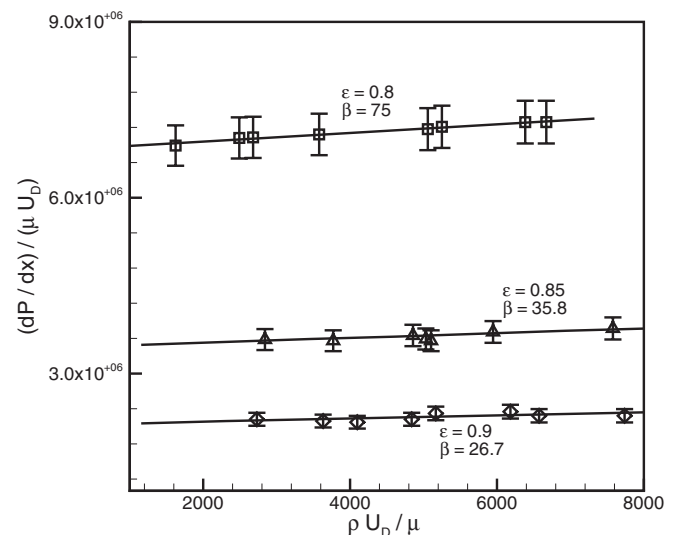


FIG. 6. Measured values of $1/\mu U_D(dp/dx)$ for the samples of tube bank with square fiber arrangement.

TABLE II. Uncertainty in the measured parameters.

Parameter	Uncertainty
ρ	3%
$\Delta P/L$	1% of full scale
Q	4% of full scale
U_D	4%
K	12%
β	12%

where

$$\frac{E(\rho U_D/\mu)}{\rho U_D/\mu} = \sqrt{\left[\frac{E(\rho)}{\rho}\right]^2 + \left[\frac{E(U_D)}{U_D}\right]^2 + \left[\frac{E(\mu)}{\mu}\right]^2}, \quad (11)$$

$$\frac{E(\Delta P/L\mu U_D)}{\Delta P/L\mu U_D} = \sqrt{\left[\frac{E(\Delta P/L)}{\Delta P/L}\right]^2 + \left[\frac{E(U_D)}{U_D}\right]^2 + \left[\frac{E(\mu)}{\mu}\right]^2}. \quad (12)$$

$E(\cdot)$ is the uncertainty in measurement of each parameter; these values are listed in Table II. The maximum uncertainty in the experimental values of permeability and inertial coefficient is estimated to be 12%.

V. NUMERICAL PROCEDURE

Equations (6) and (7) are solved using FLUENT [45] which is a finite volume based software. The second order upwind scheme is selected to discretize the governing equations and the SIMPLE algorithm [46] is employed for pressure-velocity coupling. The inlet and outlet boundaries of the computational domains are considered to be periodic, i.e., the velocity distributions on both boundaries are the same [45]. The symmetry boundary condition is applied on the side borders of the considered unit cells; this means that the normal velocity and gradient of the parallel component of the velocity on the side borders are zero. Structured grids and unstructured grids are generated for 1D, 2D, and 3D networks, respectively, using GAMBIT [45], the preprocessor in FLUENT software.

Numerical grid aspect ratios are kept in the range of 1–7. Grid independence is tested for different cases and the size of the computational grids used for each geometry is selected such that the maximum difference in the predicted values for pressure gradient is less than 2%. The maximum number of grids used for 1D and 2D-3D structures are approximately 14k and 1400k, respectively. It should be noted that the convergence criterion, the maximum relative error in the value of dependent variables between two successive iterations, is set at 10^{-6} .

In the present study, numerical simulations are carried out for fibrous networks in the porosity range of 0.3–0.95 and in the Reynolds number range of 0.001–200. SC arrangements are orthotropic while the rest of the considered structures are anisotropic [10]. Therefore, numerical simulations are conducted for flow parallel to different coordinate axes. The same method as described in the previous section is employed to determine the permeability and the inertial and/or

TABLE III. Flow properties for the considered fibrous structures.

Square array (1D)					
Normal flow			Parallel flow		
ε	K/d^2	F	ε	K/d^2	F
0.45	0.0015	0.13	0.45	0.0079	0
0.65	0.014	0.026	0.55	0.0177	0
0.8	0.072	0.018	0.65	0.0378	0
0.9	0.300	0.011	0.8	0.1667	0
0.95	0.892	0.009	0.9	0.643	0
Planar structures (2D)					
Through-plane flow			In-plane flow		
ε	K/d^2	F	ε	K/d^2	F
0.35	0.0007	0.313	0.35	0.0016	0.092
0.5	0.0046	0.118	0.5	0.0069	0.046
0.6	0.012	0.091	0.6	0.0164	0.033
0.8	0.106	0.033	0.8	0.0807	0.018
0.9	0.439	0.0028	0.9	0.4119	0.013
Simple cubic (3D)					
ε	K/d^2	F			
0.31	0.0011	0.914			
0.37	0.0023	0.562			
0.59	0.0174	0.141			
0.79	0.118	0.041			
0.87	0.336	0.024			

Forchheimer coefficient from numerical results for different unit cells. The summary of the computed flow coefficients is reported in Table III.

Flow parallel to axes of square arrays of cylinders is similar to laminar channel flows. This leads to zero value for Forchheimer coefficient in parallel flow as reported in Table I. Similarly, for 2D structures, the in-plane Forchheimer coefficients have lower values than the calculated values for through-plane flow. This results from the fact that 50% of the fibers in the considered geometry are parallel to the flow direction. Therefore, no inertial drag forces are exerted on these fibers.

VI. COMPARISON OF THE NUMERICAL RESULTS WITH EXISTING DATA IN THE LITERATURE

A. Square arrangement (1D)

To verify the numerical analysis, in Fig. 7, the calculated values of the dimensionless normal permeability, K/d^2 , are successfully compared with present experimental results and the data collected from several sources [47–52]. Moreover, in Fig. 8, the calculated Forchheimer coefficients for square arrangements are compared with the present experimental data, the numerical results of Ghaddar [39] and Papatnasiou *et al.* [40] for monodisperse and bimodal fiber arrays, respectively. In addition, the experimental data of Bergelin *et al.* [47] (oil flowing across tube banks) are included in Fig. 8. In

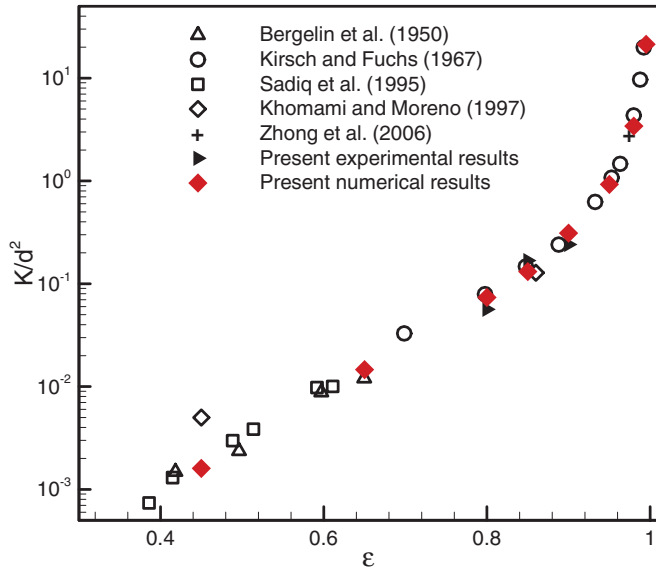


FIG. 7. (Color online) Comparison between the present numerical results, collected experimental results, and data from various sources, for normal flow through square fiber arrays.

general, the present results are in good agreement with the collected and reported data by others.

B. 2D and 3D simple cubic structures

To the best knowledge of the authors, there are no experimental data for moderate Reynolds flow through the ordered 2D and 3D structures considered in the present study. To verify our analysis, in Fig. 9, the calculated permeability values for simple cubic arrangement are successfully compared with the numerical results of Higdon and Ford [32] and experimental data for actual 3D materials with random

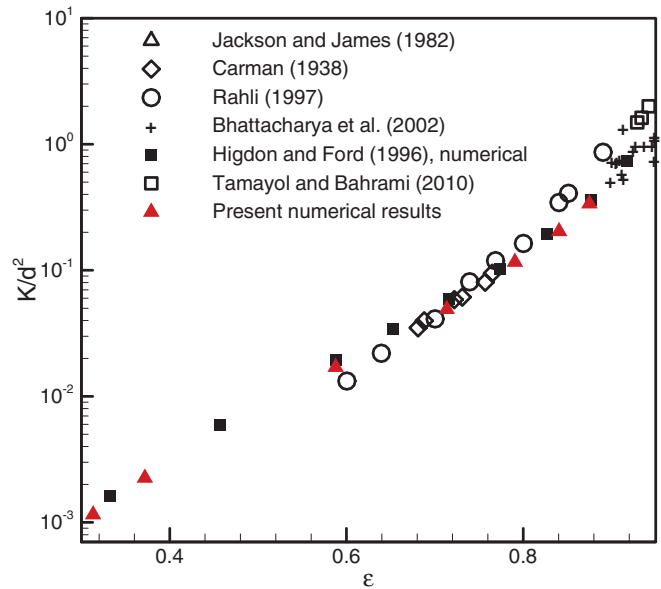


FIG. 9. (Color online) Comparison between the present numerical results for permeability of simple cubic arrangements with existing numerical and experimental data of 3D materials.

fiber distribution collected from different sources. The plotted data are based on permeability results for polymer chain in solutions [53], glass wool randomly packed [54], stainless steel crimps [22,54], metallic fibers [55], and aluminum metal foams [29,56].

VII. EFFECTS OF MICROSTRUCTURE ON FLOW PROPERTIES

Effects of microstructure and more specifically fibers orientation on permeability and Forchheimer coefficient are investigated in Figs. 10 and 11, respectively. As expected,

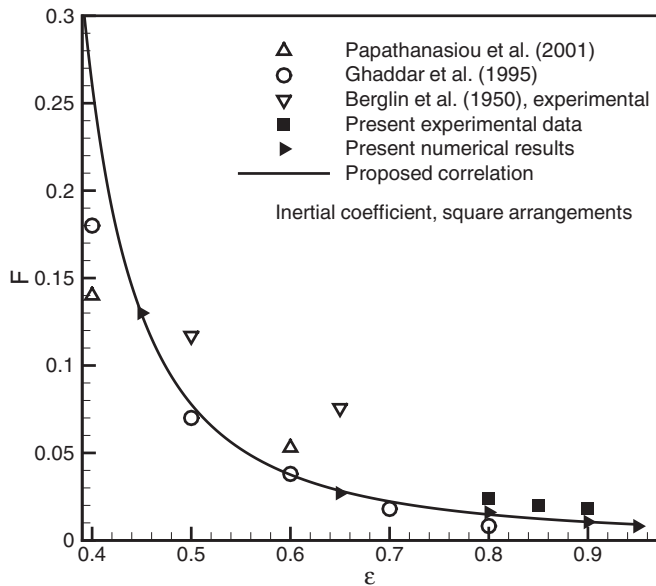


FIG. 8. Comparison between the present numerical and experimental results for Forchheimer coefficient with experimental and numerical data of others.

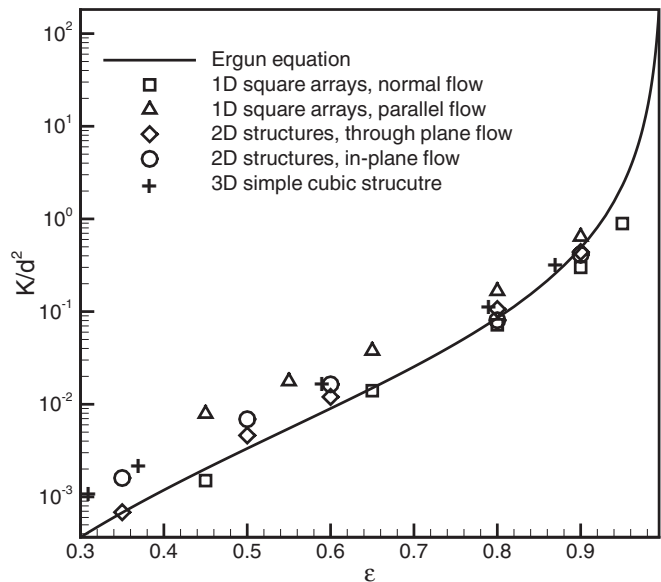


FIG. 10. Comparison of numerical values of dimensionless permeability of fibrous media with Ergun equation.

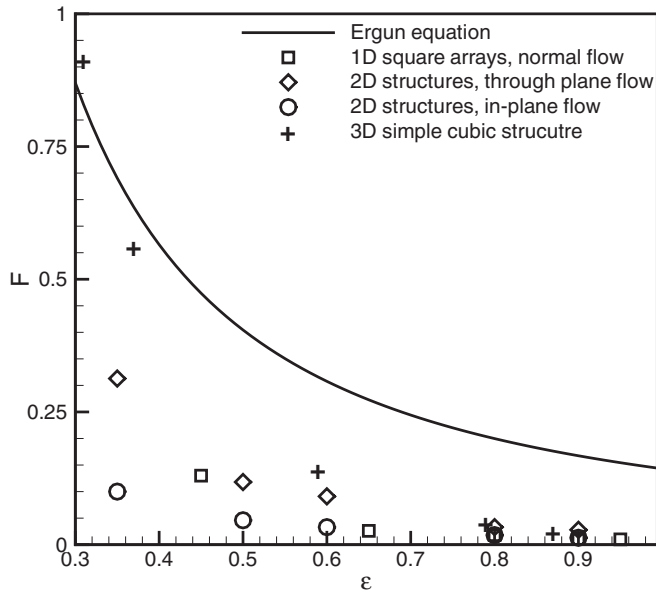


FIG. 11. Comparison of numerical values of Forchheimer coefficient of fibrous media with Ergun equation.

1D arrangements are the most anisotropic geometry and the normal and parallel permeability of such structures provide the lower and upper bounds for permeability of fibrous media. Effects of microstructure are more pronounced in lower porosities.

As discussed in previous sections, 1D and 2D geometries are anisotropic; this can also be observed in the plotted data in Fig. 11. In addition, the Forchheimer coefficient for 3D structures is higher than values for 1D and 2D geometries. The Forchheimer coefficient, which is a reflection of inertial effects, is more influenced by microstructure in the porosity range of $\varepsilon < 0.7$.

The Ergun equation (9), is a widely accepted equation for prediction of pressure drop across granular materials. Two main differences between fibrous and granular materials are as follows:

- (1) Shape of the particles in granular materials is spherical while fibrous media are made up of cylindrically shaped particles.
- (2) Porosities of granular materials are in the range of 0.2–0.6, while the porosity of fibrous materials usually is in the range of 0.6–0.999.

The present numerical results are compared with the values predicted by the Ergun equation to figure out if this equation is applicable to high porosity fibrous structures. Figure 10 includes the predicted values of permeability from the Ergun equation and the present numerical results. It should be noted that Fig. 10 has a logarithmic scale. As such, the difference between the numerical results and the permeability values predicted by the Ergun equation are significant. However, since the viscous term in the Ergun equation is based on the capillary theory leading to the Carman-Kozeny equation [9], it qualitatively predicts the observed trends in the numerical data.

The Forchheimer results calculated from the Ergun equation are plotted against the current numerical results in

TABLE IV. Proposed correlations for Forchheimer coefficient in fibrous media.

Flow direction, microstructure	$F = (a + b\varepsilon)^{-1/c}$		
	a	b	c
Normal, square arrays (1D)	−5.32	18.42	0.532
Through plane, 2D structures	−0.14	5.05	0.418
In-plane, 2D structures	1.037	0.0863	0.025
Simple cubic arrangements (3D)	0.534	1.56	0.184

Fig. 11. The comparison shows that the inertial term in the Ergun equation is only in agreement with numerical results for 3D materials with low porosities. For higher porosities Eq. (9) is incapable of predicting the pressure drop for fibrous media. Therefore, a series of compact correlations for 1D, 2D, and 3D fibrous structures listed in Table IV is proposed instead. The proposed correlations are accurate within 2% of the present numerical results.

Using a scale analysis technique, Tamayol and Bahrami [22] proposed compact relationships for determining the permeability of various fibrous microstructures. As such, the permeability relationships reported by [22] and the correlations listed in Table IV enable one to predict the pressure drop in fibrous structures for moderate Reynolds number flows, i.e., $Re < 200$.

VIII. CONCLUSIONS

The effects of porosity and fiber orientation on the viscous permeability and the Forchheimer coefficient of monodispersed fibers were investigated. Fibrous porous materials were classified into three main categories: 1D, 2D, and 3D structures. Using a unit-cell approach, the flow through the considered geometries (1D, 2D, and 3D) were solved numerically over a wide range of Reynolds numbers ($0.01 < Re < 200$). The results were then used to calculate permeability and the inertial coefficient of the solid matrices.

An experimental study was undertaken. The permeability and the inertial coefficient in three samples of 1D tube banks with square arrangement were measured over a range of the Reynolds numbers. The numerical results for permeability and inertial coefficient were successfully compared with the present experimental results and the data collected from various sources. The results suggested that both permeability and Forchheimer coefficients were functions of porosity and fiber orientation. In addition, a comparison of the numerical results with the Ergun equation reveals that this equation was not accurate for highly porous materials. Using the numerical results, compact accurate correlations were proposed for determining the Forchheimer coefficient in fibrous media.

ACKNOWLEDGMENTS

The authors gratefully acknowledge the financial support of the Natural Sciences and Engineering Research Council of Canada, NSERC.

- [1] L. Spielman and S. L. Goren, *Environmental Science and Technology* **2**, 279 (1968).
- [2] G. A. Truskey, F. Yuan, and D. E. Katz, *Transport Phenomena in Biological Systems* (Pearson Prentice Hall Bioengineering, Upper Saddle River, NJ, 2004).
- [3] B. T. Astrom, R. B. Pipes, and S. G. Advani, *J. Compos. Mater.* **26**, 1351 (1992).
- [4] L. Tadrist, M. Miscevic, O. Rahli, and F. Topin, *Exp. Therm. Fluid Sci.* **28**, 193 (2004).
- [5] S. Mahjoob and K. Vafai, *Int. J. Heat Mass Transfer* **51**, 3701 (2008).
- [6] J. P. V. L. Orgéas, D. Favier, J. L. Auriault, and S. Le Corre, *Phys. Rev. E* **77**, 011303 (2008).
- [7] G. R. Plaza, *Phys. Rev. E* **82**, 031902 (2010).
- [8] A. Tamayol, F. McGregor, and M. Bahrami, *J. Power Sources* **204**, 94 (2012).
- [9] M. Kaviany, *Principles of Heat Transfer in Porous Media* (Springer-Verlag, New York, 1992).
- [10] M. M. Tomadakis and T. Robertson, *J. Compos. Mater.* **39**, 163 (2005).
- [11] J. Happel, *AIChE* **5**, 174 (1959).
- [12] S. Kuwabara, *J. Phys. Soc. Jpn.* **14**, 527 (1959).
- [13] H. Hasimoto, *J. Fluid Mech.* **5**, 317 (1959).
- [14] A. S. Sangani and A. Acrivos, *Int. J. Multiphase Flow* **8**, 193 (1982).
- [15] J. E. Drummond and M. I. Tahir, *Int. J. Multiphase Flow* **10**, 515 (1984).
- [16] E. M. Sparrow and A. L. Loeffler, *AIChE* **5**, 325 (1959).
- [17] B. R. Gebart, *J. Compos. Mater.* **26**, 1100 (1992).
- [18] A. Tamayol and M. Bahrami, *Int. J. Heat Mass Transfer* **52**, 2407 (2009).
- [19] A. Tamayol and M. Bahrami, *J. Power Sources* **196**, 3559 (2011).
- [20] G. W. Jackson and D. F. James, *Can. J. Chem. Eng.* **64**, 364 (1986).
- [21] M. P. Sobera and C. R. Kleijn, *Phys. Rev. E* **74**, 036301 (2006).
- [22] A. Tamayol and M. Bahrami, *Phys. Rev. E* **83**, 046314 (2011).
- [23] M. Sahraoui and M. Kaviany, *Int. J. Heat Mass Transfer* **37**, 1029 (1994).
- [24] A. S. Sangani and C. Yao, *Phys. Fluids* **31**, 2435 (1988).
- [25] S. Jaganathan, H. Vahedi Tafreshi, and B. Pourdeyhimi, *Powder Technol.* **181**, 89 (2008).
- [26] S. Jaganathan, H. Vahedi Tafreshi, and B. Pourdeyhimi, *Chem. Eng. Sci.* **63**, 244 (2008).
- [27] A. Koponen, D. Kandhai, E. Hellén, M. Alava, A. Hoekstra, M. Kataja, K. Niskanen, P. Slood, and J. Timonen, *Phys. Rev. Lett.* **80**, 716 (1998).
- [28] L. Hao and P. Cheng, *J. Power Sources* **186**, 104 (2009).
- [29] M. A. Van Doormaal and J. G. Pharoah, *Int. J. Numer. Methods Fluids* **59**, 75 (2009).
- [30] M. Palassini and A. Remuzzi, *Am. J. Physiol.: Renal, Fluid Electrolyte Physiol.* **274**, 223 (1998).
- [31] D. S. Clague, B. D. Kandhai, R. Zhang, and P. M. A. Slood, *Phys. Rev. E* **61**, 616 (2000).
- [32] J. J. L. Higdon and G. D. Ford, *J. Fluid Mech.* **308**, 341 (1996).
- [33] A. Nabovati, E. W. Llewellyn, and A. C. M. Sousa, *Composites: Part A* **40**, 860 (2009).
- [34] D. Nagelhout, M. S. Bhat, J. C. Heinrich, and D. R. Poirier, *Mater. Sci. Eng. A* **191**, 203 (1995).
- [35] A. R. Martin, C. Saltiel, and W. Shyy, *Int. J. Heat Mass Transfer* **41**, 2383 (1998).
- [36] S. L. Lee and J. H. Yang, *Int. J. Heat Mass Transfer* **40**, 3149 (1997).
- [37] D. L. Koch and A. J. C. Ladd, *J. Fluid Mech.* **349**, 31 (1997).
- [38] D. A. Edwards, M. Shapiro, P. Bar-Yoseph, and M. Shapira, *Phys. Fluids* **2**, 45 (1990).
- [39] C. K. Ghaddar, *Phys. Fluids* **7**, 2563 (1995).
- [40] T. D. Papathanasiou, B. Markicevic, and E. D. Dendy, *Phys. Fluids* **13**, 2795 (2001).
- [41] X. Rong, G. He, and D. Qi, *Chemi. Eng. Commun.* **194**, 1 (2007).
- [42] K. Boomsma, D. Poulikakos, and Y. Ventikos, *Int. J. Heat Fluid Flow* **24**, 825 (2003).
- [43] C. L. Tucker III and E. Liang, *Compos. Sci. Technol.* **59**, 655 (1999).
- [44] Z. Xia, Y. Zhang, and F. Ellyin, *Int. J. Solids Struct.* **40**, 1907 (2003).
- [45] *FLUENT 6.3 Users' Guide* (Fluent, Inc., Lebanon, NH, 2007).
- [46] H. K. Versteeg and W. Malalasekera, *An Introduction to Computational Fluid Dynamics* (Longman Scientific and Technical, New York, 1995).
- [47] O. P. Bergelin, G. A. Brown, H. L. Hull, and F. W. Sullivan, *ASME Trans.* **72**, 881 (1950).
- [48] A. A. Kirsch and N. A. Fuchs, *Ann. Occup. Hyg.* **10**, 23 (1967).
- [49] T. A. K. Sadiq, S. G. Advani, and R. S. Parnas, *Int. J. Multiphase Flow* **21**, 755 (1995).
- [50] B. Khomami and L. D. Moreno, *Rheol. Acta* **36**, 367 (1997).
- [51] L. Skartsis, B. Khomami, and J. L. Kardos, *Polymer Eng. Sci.* **32**, 231 (1992).
- [52] W. H. Zhong, I. G. Currie, and D. F. James, *Exp. Fluids* **40**, 119 (2006).
- [53] D. F. James and G. W. Jackson, *Biorheology* **19**, 317 (1982).
- [54] P. C. Carman, *J. Soc. Chem. Ind.* **57**, 225 (1937).
- [55] O. Rahli, L. Tadrist, M. Miscevic, and R. Santini, *J. Fluids Eng.* **119**, 188 (1997).
- [56] A. Bhattacharya, V. V. Calmidi, and R. L. Mahajan, *Int. J. Heat Mass Transfer* **45**, 1017 (2002).